IET Generation, Transmission & Distribution

IET The Institution of Engineering and Technology WILEY

ORIGINAL RESEARCH PAPER

A modified droop control structure for simultaneous power-sharing and DC voltage oscillations damping in MT-HVDC grids

Neda Azizi[1] | Hassan Moradi CheshmehBeigi[1] [iD] | Kumars Rouzbehi[2]

[1] Department of Electrical Engineering, Razi University, Kermanshah, Iran

[2] Department of System Engineering and Automatic Control, University of Seville, Seville, Spain

Correspondence
Hassan Moradi CheshmehBeigi, Tagh-e-Bostan, University St., Kermanshah, Iran.
Email: ha.moradi@razi.ac.ir

Abstract

With increasing energy demand, the use of renewable energy resources is increasing. Renewable energy sources require power electronic converters to get integrated into power grids. Multi-terminal high voltage direct current (MT-HVDC) systems are a promising solution for their grid integration. Using droop-based controller strategies in power converter stations of MT-HVDC grid, in addition, to providing power-sharing, can support the frequency of the connected AC grids. However, power changes lead to direct voltage deviations, thereby disrupting the stability of the MT-HVDC system. Here, a new control structure for the droop controller of the voltage source converter (VSC) controller is proposed which is named modified droop controller (M-Droop). This method, in addition to power-sharing, uses an appropriate control action to provide the required voltage stability. Here, analytical studies of the modified control strategy are reported. Moreover, through a developed MATLAB Simulink platform, its performance is verified in the events of transients, consisting of fault, variable load, and change in power generation.

1 | INTRODUCTION

One of the most important challenges on the road of multi-terminal HVDC grid development is protecting the system against DC faults. The capacitive behaviour of HVDC cables and their relatively low impedances leads to a significant increase in fault currents. DC circuit breakers (DCCBs) are one of the most effective tools for fast fault isolation [1]. Despite developments in DCCB technology, still they need to large DC reactors to reduce the rate of rising fault currents [2]. Capacitor and DC reactor connected to HVDC grid and inductance and capacitance of HVDC transmission lines make a kind of LC filter, which seriously affects the dynamic response of DC link voltage and its instantaneous power in MT-HVDC grid, especially in the long lines [3]. The main contest in control of MT-HVDC grids is direct voltage regulation with low capacitance [3]. The available control methods for solving this challenge include two options. The first option is based on the central controller and the second option is known as the decentralized method. In the first option, the entire system is monitored through an external communications link and the controller delivers the

optimal power flow for the system's resources and load. The advantage of this method is that it is optimal, and its major disadvantage is its dependence on external communications [4]. In addition, the implementation of the proposed method in the MT-HVDC grid reduces transient voltage oscillations. However, the control strategy of the second option includes methods such as droop [5], master-slave [6], and DC bus signalling method [7]. In [8], droop control methods are proposed based on the decentralized methods, but most of them cannot deliberate the influence of the resistance of cable and errors of sensor gain. Moreover, there is a trade-off between voltage regulation and current sharing in these methods. Adaptive or nonlinear droop is proposed in [8, 9], in which the trade-off between load sharing and voltage regulation is minimal, but these methods also perform poorly when the power converter current is negative or the power is reversed. Alongside with this methods, there are strategies include the combination of both centralized and decentralized methods as different control layers, which in addition to the advantages, include disadvantages of two methods [10].

In DC grids, the DC voltage has a similar role as the power balance sign that the frequency has in AC grids [11]. That is, the DC voltage dynamics are determined by the energy stored as electrostatic potential energy in the capacitors in the grid [12]. However, conventional droops cannot increase the capacitance. Therefore, a new control method for MMC, called virtual capacitor control, is proposed in [13], which makes it possible to reduce the DC grid oscillation by simulating the dynamic response of a physical capacitor. To perform automatic synchronization using the DC-link capacitor dynamics, the authors in [14] employed a virtual synchronous control, which mimics the synchronization feature of a synchronous generator. The most important advantage of this method is that it is operated without a phase-locked loop (PLL), and therefore avoids instability caused by the PLL when connecting the VSC to a weak grid.

The Inertia Emulation Control (INEC) algorithm proposes a method for the inertia emulation that uses the energy stored in the DC-link capacitor to mimic the inertial response of an SG, but this may need the large capacitors to be added to the system. The addition of these capacitors increases costs and will affect the dynamics of the controllers. Combined strategy is another method for emulated inertia, which utilizes both DC-link capacitor and wind turbine kinetic energy, this method is used only in a point-to-point HVDC system and requires some modifications to operate on a DC network [15]. Though for appropriate voltage regulation and power-sharing, a proper strategy is needed to enable the converter to increase DC capacitance. This paper proposes a modified droop controller (M-Droop) that provides capacitance using the energy stored in the grid where the fault occurred. The M-Droop can provide the capacitance requirement of the HVDC grid without depending on frequency measurement and PLL. The contributions of this study are:

- This paper proposes a successful method for simultaneous power-sharing and oscillations of DC voltage damping
- The proposed method does not require increasing the value of DC-link capacitors
- As the conventional DC-PSS can only neutralize a small part of the voltage fluctuations, while, given the presence of the droop controller on the system, it has no proper effect on the volatility of the power. This study shows that the M-droop controller also provides a part of the capacitance required by the system in addition to damping of the direct voltage oscillations.

The rest of this paper is organized as follows: Conventional droop controller performance is expressed in Section 2. Section 3 is built based on the proposed control strategy. The understudy network and its modelling are discussed in Section 4. The optimization approach is investigated in Section 5. Dynamic performance analysis is analysed in Section 6. Simulations verify and confirm the analytical analysis described in Section 7. Finally, conclusions are given in Section 8.
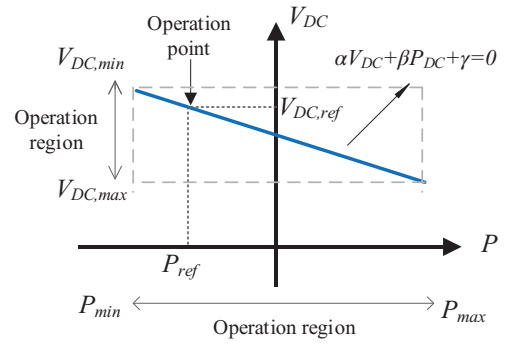

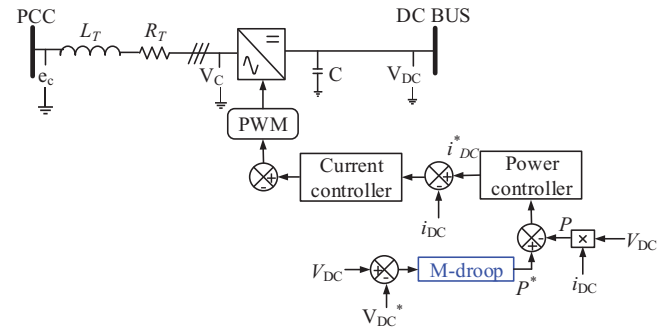**FIGURE 1**   Generalized characteristics of the proposed droop controller

FIGURE 2   Control structure of the proposed controller for a VSC station

2 | PERFORMANCE OF A CONVENTIONAL DROOP CONTROLLER

Figure 1 demonstrates the general characteristics of the droop controller.

Usually, $P*$ as the active power reference is manipulated by the voltage droop controller ($V–P$), so, the active power control scheme acts as part of the plant of droop control model.

The coefficient of the droop characteristics can be calculated according to the power flow results [4, 16] or grid condition and stability [17].

3 | PROPOSED CONTROL STRATEGY

The main contest in control of MT-HVDC grids is direct voltage regulation with low capacitance [3].

This paper suggests a method to provide the transient damping for direct voltages of the HVDC grid during the transient conditions. In this structure, the M-droop controller supplementary signal is being used instead of the conventional $V–P$ droop controller to increase the stability of the HVDC grid. Figure 2 shows a general structure of a proposed controller for a VSC station. The configuration of the proposed M-droop controller is revealed in Figure 3. Since the measured local voltage is known as the power balance indicator in the HVDC grid, in this structure, the locally measured voltage is used as the input signal. This M-droop provides an auxiliary capacitance. In
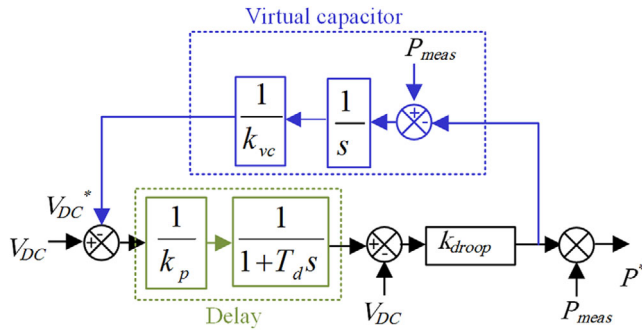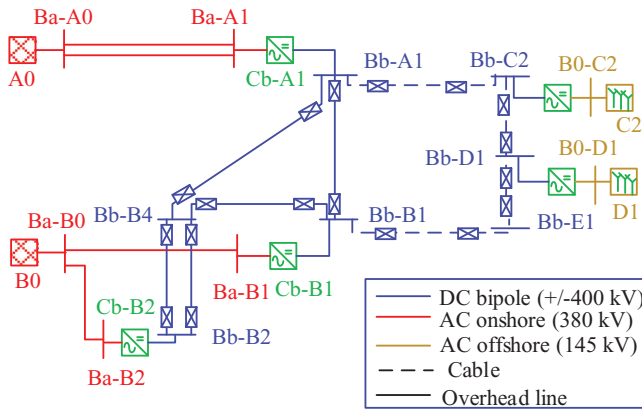
FIGURE 3 M-droop control structure

FIGURE 4 Cigre DCS3 test MT-HVDC grid

addition, to filter noises in the measured output power of the V–P droop controller, a low pass filter is usually added to the structure.

3.1 | Virtual capacitor control

Inertia in an AC system is defined as the system's ability to prevent sudden events of frequency. In general, H_s is defined as the ratio of stored kinetic energy (E_k) and the rated power (S_n), as presented in (1):

$$H_s = \frac{E_k}{S_n} \qquad (1)$$

Inertia constant can be defined as (2) [18]:

$$H_{dc} = \frac{W_k}{S_{VSC}} \qquad (2)$$

where W_k is stored energy in capacitors and S_{VSC} is the rated power of VSC. Compared to synchronous generators with the same capacity, the H_{dc} is small. However, this value can be increased by increasing the capacitance of the DC link capacitor, but this increases the cost and short circuit level and reduces the dynamic characteristics of the DC bus [19].

The dynamic response of a DC capacitor is defined as (3):

$$C_{DC} V_{DC} \frac{dV_{DC}}{dt} = P_i - P_o = \Delta P_{DC} \qquad (3)$$

where P_o is the output power and P_i is the input power. Due to the high speed and flexibility of the VSC controller, the additional power ΔP_{VSC}, considering the range of direct voltage change, can be obtained through the active power control.

$$\Delta P_{VSC} = \frac{C_{vir} V_{DC}}{S_{VSC}} \frac{dV_{dc}}{dt} \qquad (4)$$

With the participation of additional power, the DC link capacitor dynamics change as follows.

$$C_{DC} V_{DC} \frac{dV_{DC}}{dt} + C_{vir} V_{DC} \frac{dV_{DC}}{dt} = P_{i(pu)} - P_{o(pu)} \qquad (5)$$

According to (5), the additional power ΔP_{VSC} obtained through power control can produce a virtual capacitor. This capacitor provides more inertia to support direct voltage.

In this study, additional power is obtained through the remaining power of the system after the power-sharing or fault.

The operation of the grid controllers is such that after power-sharing or at the time of the fault, the grid may be in a situation where the power reference of the converters is not at maximum power.

In this case, part of the grid power can be stored as additional power.

3.2 | M-Droop controller

A design characteristic of the modified droop controller is shown in (6), and (7) indicates the value of the droop coefficient of this new controller.

$$P_w = P_{w,ref} - k_1 \left(V_{DC} - V_{DC,ref} \right) + k_{vc} V_{DC} \qquad (6)$$

$$k_{vc} = k_2 \frac{dV_{DC}}{dt} \qquad (7)$$

As shown in (6), if the direct voltage remains constant, the proposed droop controller converts to the conventional droop controller, where P_w is the nominal value of power.

$$P_w^* = P_{w,ref} - k_1 \left(V_{DC,ref} - V_{DC} \right) \qquad (8)$$

Comparing (6) with (8),

$$P_w = P_w^* + k_{vc} V_{DC} \qquad (9)$$

Regardless of the power losses, it can be said that the output power P_{out} is equal to the injected power P_i.

By considering the droop controller in the system, power changes can be written as (10), where, P_c is the power of the

converter without droop controller effect.

$$P_i = P_{out} = P_c - k_w \left(P_w - P_{w,ref} \right) \tag{10}$$

Substituting (9) into (10) yields:

$$P_i = P_c - k_w \left(P_w^* - P_{w,ref} \right) - k_W k_{vc} V_{DC} \tag{11}$$

According to (3), (12) can be written as follows:

$$C_{DC} V_{DC} \frac{dV_{DC}}{dt} = \underbrace{P_c - k_w \left(P_w^* - P_{w,ref} \right)}_{P_{in}} - k_W k_{vc} V_{DC} - P_o \tag{12}$$

$$P_o - P_{in} = C_{DC} V_{DC} \frac{dV_{DC}}{dt} - k_w k_2 V_{DC} \frac{dV_{DC}}{dt} \tag{13}$$

Therefore, the above equations show that using power changes, the droop controller can be designed in a way that to be able to emulate the behaviour of the virtual capacitor. Therefore, the proposed method does not require increasing the value of DC-link capacitors. In addition, according to (13), it can be said that the capacity of the virtual capacitor is equal to (14):

$$C_{vir} = k_w k_2 \tag{14}$$

3.3 | Effects of delays

There are always delays in MT-HVDC grids [20]. Usually, in the structure of a droop control, a low pass filter is added to filter noises in the measured output power. Assuming this delay is first-order lags with a time constant T_d and a gain $1/kp$ has to be replaced by $1/(1 + Td\,s)$ in the small-signal models.

4 | UNDERSTUDY NETWORK AND ITS MODELING

In order to investigate the proposed control strategy, the grid that is shown in Figure 4 is selected. In this grid 5-terminal bipolar MT-HVDC grid are connected to four AC areas connected.

The test grid is formed by two onshore AC systems, two offshore AC systems, and five VSC-HVDC converters. It is worth noting that the typical test grid (Cigre DCS3) has been selected only as a selective test case, and the proposed scheme can be easily selected in other VSC-based HVDC grids.

The main goal in the current paper is to improve the stability of the DC voltage and reduce variations of power in the states of transients, and this standard grid is selected to approve the performance and appropriateness of the proposed control method.

In this paper, transmission lines are modelled by the frequency-dependent π (FD-π) section modelling [21] that consists of multiple cascaded π sections which are represented by series RL circuits, and shunt capacitors C [4].

Eigen value-based analysis of small signal dynamics in HVDC transmission systems requires cable models that are compatible with the display of state space. While distributed parameter models that calculate frequency-dependent effects are inherently inconsistent with the display of state space, a typical π model can only accurately show cable behaviour at a frequency.

Instead, a FD-π model, consisting of a lumped circuit representation with multiple parallel RL-branches in each π-section can be utilized to reproduce the frequency dependency of the cable characteristics in a specified frequency range.

So, the number of sections and parallel branches are considered as follows: $n = 10$, $m = 5$. Moreover, the rated power of each converter is 1000 MW and the rated voltage is ±320 kV. It is also assumed that the topology of the understudy system is a symmetrical monopole topology.

According to the results obtained in [22], Ba-B1 has been selected as the appropriate location for M-droop placement.

5 | OPTIMIZATION APPROACH

The parameters of the M-droop controller must be adjusted to decrease the objective function (15).

$$Error = \sum_{b=1}^{n} \left(M_{V_b} \right) \tag{15}$$

where M_{V_b} is the maximum peak of direct voltage oscillations from reference value for n DC bus in fault time is visible in (15). It should be noted that in this paper $n = 5$.

This equation confirm that, without any fault or malfunction in the system, the Error function will be zero. In this paper, the particle swarm optimization (PSO) algorithm and genetic algorithm (GA) are employed to determine the parameters of M-droop based on (15). The optimum parameters are obtained with 110 repetitions following four scenarios include:

- Case 1: Three-phase to ground in Ba-A0 with a duration of 15 ms.
- Case 2: Three-phase to ground in Ba-B0 with a duration of 15 ms.
- Case 3: Three-phase to ground in Ba-A0 with a duration of 10 ms.

Optimization results for the M-droop controller obtained by PSO and GA are shown in Table 1.

The procedure of optimization of parameters in this paper is expressed in the following levels.

Level 1. The population is set.

TABLE 1 Optimization results for M-droop controller obtained by PSO algorithms

	Parameter	Optimal valuePSO	Optimal valueGA
Case 1	k_1	1.9	1.83
	k_2	4.3	4.51
	k_w	31.5	30.9
	k_p	0.019	0.0188
Case 2	k_1	1.85	1.9
	k_2	4.2	4.16
	k_w	30.1	30.2
	k_p	0.024	0.026
Case 3	k_1	1.81	1.85
	k_2	4.4	4.31
	k_w	30.8	31.05
	k_p	0.027	0.023

Level 2. At first, a particle is selected and the value of each parameter is calculated based on this particle. Then, the minimum and maximum limits for each parameter are checked, and finally, the E_{rror} criterion is calculated at this level.

Level 3. At this level, the position (parameter) of each particle compares with its previous value, and the better particle is selected.

Level 4. The degree of adaptive aggregation and the evolution rate is calculated and the speed and position data for each particle is updated.

Level 5. In this level, if the repetition of irritation or the desired fitness corresponds to the stop criterion, the criterion stops according to the maximum number of repetitions of irritation or the desired fitness. Otherwise, it goes to the previous level.

Level 6. Otherwise, the designed parameters are verified as results.

In PSO algorithm, any particle has the situation and the speed that determined by X and V. Then, the next position and velocity of each particle during the optimization process is calculated according to the current velocity and position and the desired individual position according to (16) and (17).

$$V_i^{iter+1} = wV_i^{iter} + c_1.r_1.(P_{besti} - X_i^{iter}) + c_2.r_2.(G_{best} - X_i^{iter})$$

$$(16)$$

$$X_i^{iter+1} = X_i^{iter} + V_i^{iter+1} \tag{17}$$

where, the ith particle in the swarm is indicated by i. i_{ter}, shows iteration. Ps reveals the best position of the ith particle. G_{besti} indicates the best general situation among the swarm. w represents the weight of inertia and r_1 and r_2 are selected as random numbers between one and zero.
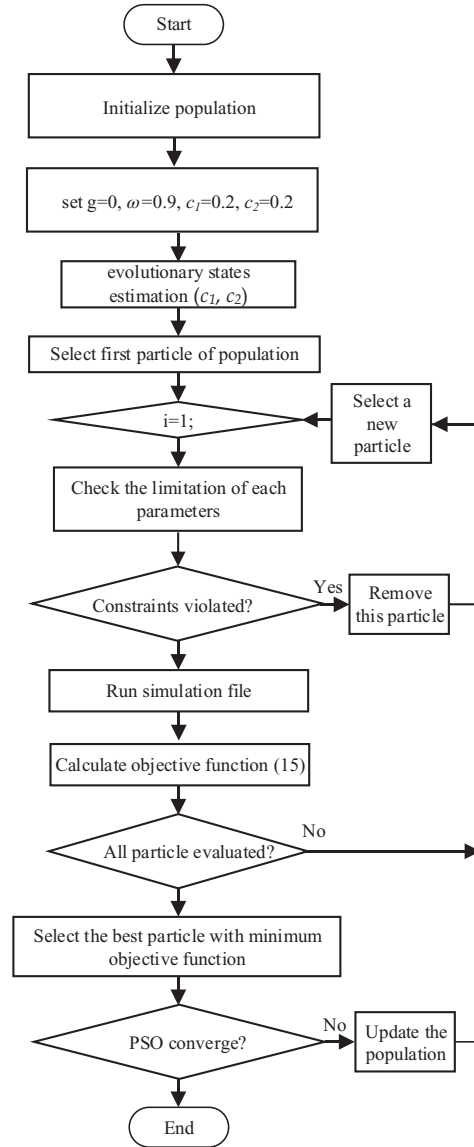

FIGURE 5 Adaptive parameters control process

In this algorithm, the updated linear inertia weight is directly related to the linear decrease in inertial weight (LDW) with increasing repetition time. However, the relationships between inertia weight and repetition time are not always the same for different optimization problems.

Figure 5 shows the flowchart of the PSO algorithm for parameters of the controller.

The parameters calculated by both algorithms are almost identical, however, the PSO algorithm reaches the final answer in less time.

6 | DYNAMIC PERFORMANCE ANALYSIS

In this part of the paper, the effect of the proposed method on system stability will be evaluated. Generally, the linearized model
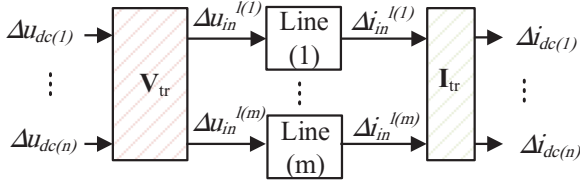
FIGURE 6 HVDC grid model integrating line models
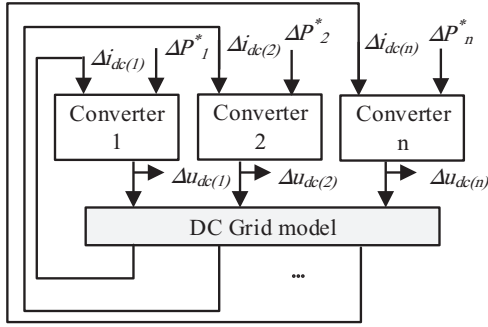

FIGURE 7 Schematic of a MIMO plant model for the DC voltage control in MT-HVDC grid

of the system in the state space form can be expressed as (18) [23].

$$\Delta \dot{x} = A\Delta x + B\Delta u \tag{18}$$

where Δu and B denote the input vector and input matrix respectively, Δx and A denote the state vector and the state space matrix respectively.

It is necessary to mention, here, the average model of VSC is used to model the power converters and the π-section model is used to model the transmission lines. The number of sections of each transmission line in the π-section model is assumed to be five to achieve the appropriate accuracy. It is also assumed that the proposed controller is located on the Cb-B2 bus.

Figure 6 displays the construction of a DC network with n converters and m lines. A schematic of a plant model of the direct voltage control in the MT-HVDC grid for stability investigation in the MT-HVDC grid is shown in Figure 7.

This model can be used for studies on a multi-input-multi-output control network (MIMO), and to study the closed-loop system following grid conditions. As shown in Figure 7, the input of the controllers of all converters is power. However, for converters equipped with a droop control system, power references in DC voltage control mode are used as the manipulated input. Power changes for converters that are in active power control mode act as a disturbance in DC voltage control. Also, the "reference" of power for each wind farm is the mechanical power taken by the turbine system.

Figure 8 illustrates the average modelling of a VSC station. As shown in Figure 8, the VSC station is modelled as a
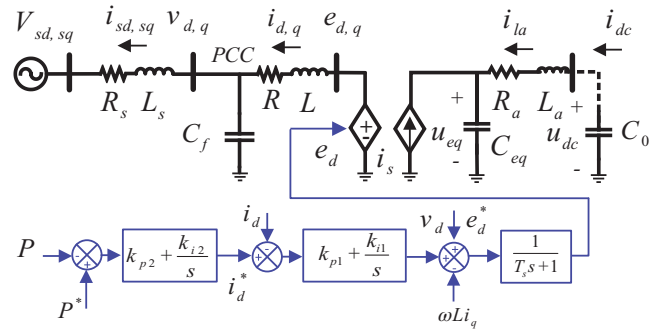

FIGURE 8 VSC-HVDC station model including its control structure

controlled voltage source on the AC side and controlled current source on the DC side behind a capacitor based on the power balance principle commonly used for modular multilevel converters (MMCs) [24].

The VSC station is operated in a *dq* synchronous reference frame. Since in the stiff AC power system, reactive power control and *q* axis current have an insufficient effect on the active power, meanwhile the *q*-axis of the voltage of PCC is generally kept on zero by the phase-locked loop (PLL) [25].

Thus, the analytical model for direct voltage stability study focuses on *d*-axis related controllers, because the purpose of the analysis is not to deal with weak systems.

The dynamics of the system linked to the *d*-axis current is shown as follow:

$$\frac{d\Delta i_{s-d}}{dt} = \omega\Delta i_{s-q} + \frac{1}{L_s}\Delta v_d - \frac{1}{L_s}\Delta v_{s-d} - \frac{R}{L_s}\Delta i_{s-d} \tag{19}$$

$$\frac{d\Delta i_d}{dt} = \omega\Delta i_q + \frac{1}{L}\Delta ve_d - \frac{1}{L}\Delta v_d - \frac{R}{L}\Delta i_d \tag{20}$$

where Δ is employed for the linearized operating point, $(R_s + j\omega L_s)$ is the grid impedance, $(R + j\omega L)$ is equivalent to the impedance of the transformer and the impedance of the reactor arm, also, ω is the velocity angular. The system dynamics of the *d*-axis filter bus voltage is expressed as (21). In this paper, the q-axis PCC voltage is properly controlled by the PLL, since, the assumption is that the VSC station is connected to a strong system. Consequently, the small-signal method of the inverting power of the VSC can be expressed by way of (22):

$$\frac{d\Delta v_d}{dt} = \omega\Delta v_q + \frac{1}{c_f}\Delta i_d - \frac{1}{c_f}\Delta i_{sd} \tag{21}$$

$$P = V_d i_d + V_q i_q \rightarrow \Delta P \approx v_{do}\Delta i_d + i_{do}\Delta v_d \tag{22}$$

The value of equivalent converter capacitor C_{eq} is adopted to the total energy stored in the MMC sub-modules. L_a as equivalent arm inductance is modeled in the DC side given by $L_{arm} = (2/3)L$ for the average model of MMC. It is assumed that the power on the AC side is equal to the power on the DC side in the PCC, the linear dynamic of DC-link capacitance can

be expressed as:

$$\frac{d\Delta u_{eq}}{dt} = \frac{\Delta i_{la}}{C_{eq}} - \frac{P_o}{C_{eq} u_{eqo}} \Delta P + \frac{P_o}{C_{eq} u_{eqo}^2} \Delta u_{eq} \quad (23)$$

The subscript "o" shows the operating point. The DC voltage u_{dc} that across C_{eq} and L_a is the voltage to be controlled voltage. To simplify the sophisticated model, a very small C_o capacitance has been modeled to enable u_{dc} to become a state variable.

$$\frac{d\Delta i_{la}}{dt} = \frac{\Delta u_{dc}}{L_a} - \frac{\Delta u_{eq}}{L_a} - \frac{R_a}{L_a} \Delta i_{la}$$

$$\frac{d\Delta u_{dc}}{dt} = -\frac{\Delta i_{la} - \Delta i_{dc}}{C_o} \quad (24)$$

The dynamic behaviour of the PI controllers related to the i_{d} and active power control is defined in (25), while the state variables of the integrators are the x_{P} and x_{id}.

$$\frac{d\Delta x_P}{dt} = -k_{i2} (\Delta P - \Delta P^*)$$

$$\frac{d\Delta x_{i_d}}{dt} = -k_{i1} (\Delta i_d - \Delta i_d^*) \quad (25)$$

The reference of i can be indicated in (26), based on the Equation (10) and the structure of the active power controller.

$$\Delta i_d^* = -k_{p2} \left[(v_{do} \Delta i_d + i_{do} \Delta v_d) - \Delta P^* \right] + \Delta x_p \quad (26)$$

The VSC modulation control is shown by a first-order transfer function with τ as a time constant. To facilitate mathematical modeling, (27) is used, which causes the AC voltage e_{d} to be converted into a state variable. The dynamics of the state variable shown in (27).

$$\frac{1}{\tau_s} \left[\Delta v_d - \omega L \Delta i_q + k_{p1} \left(\Delta i_d^* - \Delta i_d \right) + \Delta x_{id} \right]$$

$$-\frac{1}{\tau_s} \Delta e_d = \frac{d\Delta e_d}{dt} = \frac{1}{\tau_s} \left(\Delta e_d^* - \Delta e_d \right) \quad (27)$$

Here, the reference of voltage Δe_{d}^* based on the current controller construction is deliberated. To achieve the final space-state formula it is necessary to replace Δi_d^* in (27) with (26). The equivalent state variables are described as shown in (28). The matrices related to $\Delta v_{\mathrm{dc(j)}}$ and $\Delta i_{\mathrm{dc(j)}}$ are mined to enable the integration of the VSC model and the HVDC grid model as it shown in (29):

$$x_j = [\Delta e_d \ \Delta v_d \ \Delta i_d \ \Delta i_{sd} \ \Delta x_{id} \ \Delta x_p \ \Delta u_{eq} \ \Delta u_{dc} \ \Delta i_{la}] \quad (28)$$

$$\dot{x}_j = A_j x_j + B_{dj} x d_j + \begin{bmatrix} B_{jG} & B_j \end{bmatrix} \begin{bmatrix} \Delta i_{dc(j)} \\ \Delta P_j^* \end{bmatrix}$$

$$\Delta u_{dc(j)} = C_{jG} x_j \quad (29)$$

The dominant poles and zeros of the plant model $V_{DC}(s)/P^*(s)$ of direct voltage control are shown in Figure 9.

Figure 9 demonstrations the poles and zeros diagram of the model of small-signal control with the proposed controller and conventional controller.

As shown in Figure 9, the understudy grid is stable normally and entire of zeros and dominant poles are on the left side of the complex plane. Also, as shown by the direction of the arrows in the figure, the dominant poles of the system, marked in blue and corresponding to employing the M-droop, are farther away from the origin coordinates, indicating that the grid using M-droop has more stability. However, the predominant red poles associated with the conventional droop system have poles closer to the origin of the coordinates. This figure shows that by employing the M-Droop controller, poles and zeros, move farther from the vertical axis. Therefore, it can be said that the system with the M-droop controller is more stable than the system with a conventional droop controller.

Figure 10 compares the frequency response of the system with the M-Droop controller and with the conventional controller. It is clear that M-Droop gives a higher phase margin and it is more flexible. Therefore, this result confirms that the system with the M-droop controller is more stable than the system with a conventional droop controller.

7 | SIMULATION RESULTS

In this section, three different strategies are simulated on the Cigré DCS3 grid to demonstrate the advantages of the proposed M-droop strategy including conventional droop controller and M-droop controller.

Three scenarios that are discussed below consist of reducing and increasing the power output of the Cb-A1 bus at 3 s and a three-phase short at the AC side of the Cb-A1 bus for 150 ms (3–3.15 s). In these simulations, the M-Droop controller
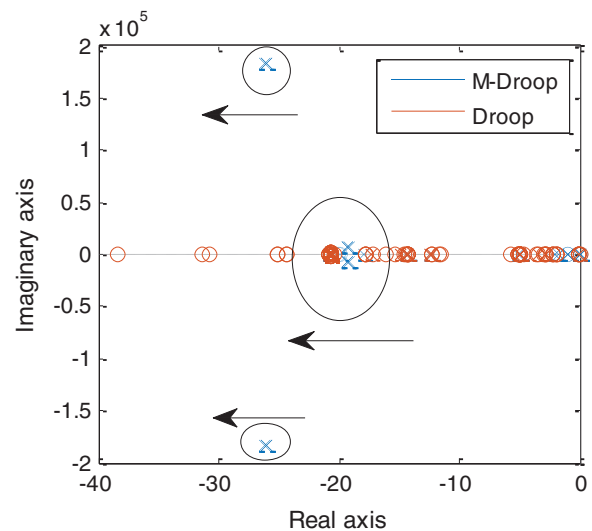

FIGURE 9 The dominant poles and zeroes of the open-loop TF $V_{DC}(s)/P^*(s)$
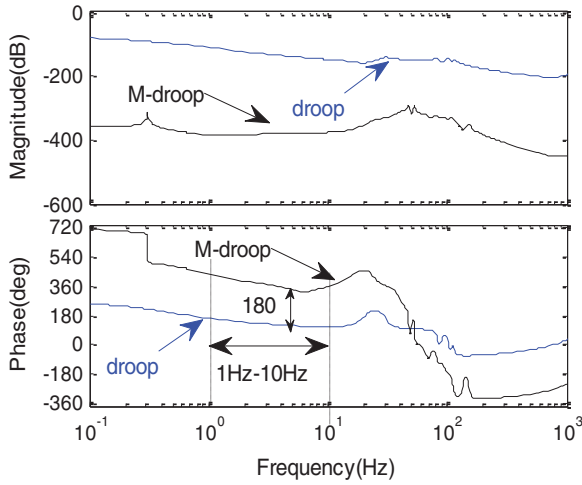
FIGURE 10 Frequency response of the open-loop TF $V_{DC}(s)/P^*(s)$

TABLE 2 Parameters of VSC-HVDC link

Parameter	Value
Total number of capacitor (N)	1
DC capacitor (C_{DC})	7 mF
Rated DC voltage of VSC (V_{DC0})	1 p.u.
Rated frequency (f_o)	50 Hz
Nominal power	1200 KVA
Nominal AC voltage	380 kV
Nominal DC voltage	400 kV
α	1
B	0.03
Γ	−0.945
$T_d(s)$	1.1 ms

FIGURE 11 (a) DC voltage and (b) power of Cb-A1, Cb-B1, Cb-B2, Cb-C2, and Cb-D1 following 250 MW reducing wind farm 2 generation

is applied to the Cb-B1 bus converter assuming the data are following Table 2.

The simulation results for Cb-A1, Cb-B1, Cb-B2, Cb-C2, and Cb-D1 buses are revealed. The VSC controller of the Cb-B1 and Cb-B2 bus is a droop controller and the VSC controller of Cb-C2 and Cb-D1 is a power controller.

Figure 11 shows the output direct voltage and power of Cb-A1, Cb-B1, Cb-B2, Cb-C2, and Cb-D1 following the load reduction scenario at the Cb-A1. As shown in Figure 11, by employing the proposed method, the direct voltage of buses is improved, they decrease more slowly and the much larger enhancement in DC voltage nadir are obtained. Because at the moment of system change, through capacitance improvement, the energy stored in the DC-link capacitor is used to maintain system stability. In addition, this energy in addition to not affecting the M-droop controller performance in power-sharing will increase the overall system stability.

Output DC voltage and DC power of all busses include Cb-A1, Cb-B2, Cb-B1, Cb-C2, and Cb-D1 following load increasing scenario at the Cb-A1 is shown in Figure 12. As shown
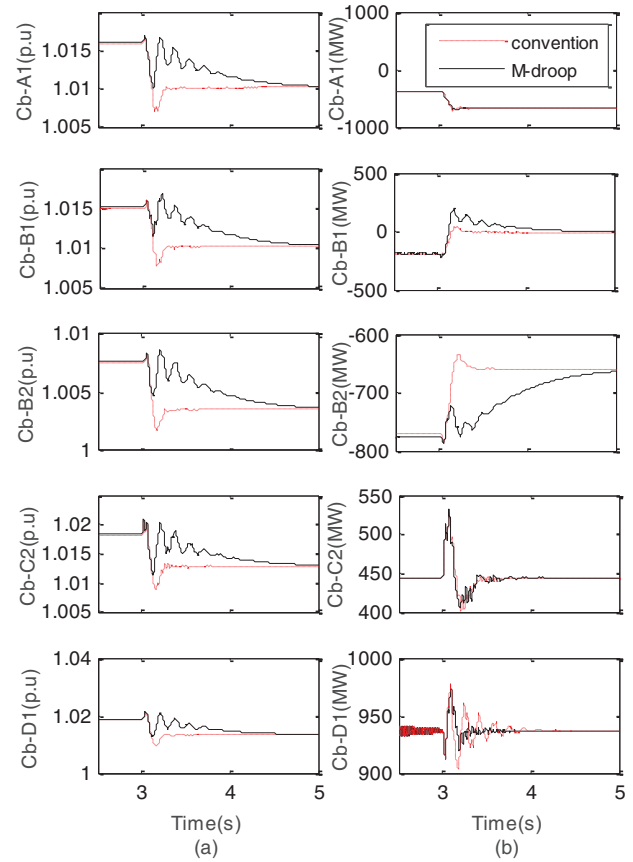
in Figure 11, with the conventional method, the direct voltage of buses, will shock and has keen sharp peaks, from the initial value to the final value. Because with the proposed method, the energy stored in the DC-link capacitor is used to maintain system stability without any affecting the performance of the droop controller.

The simulation results following the previous scenario about reducing power production for the Cb-B2 bus are shown in Figure 13 and Figure 14. The results for this bus also confirm that the stability of direct voltage of Cb-A1 and Cb-C2 can be improved by using delay filter compare M-Droop without delay filter, due to lack of drop and a sudden increase in bus voltage.

In addition, Figure 14 shows that using M-droop, bus power oscillations are also reduced and do not change abruptly. However, the system with virtual capacitor and delay filter simultaneously has less oscillation and its damping is more rapid.

Figure 15 shows the direct voltage of Cb-A1, Cb-B2, and Cb-B1 profiles during a three-phase short circuit to the ground at the AC side of the Cb-A1 bus for 150 ms (3–3.15 s).

As shown in Figure 15, with the M-droop method, the direct voltage and power of buses have smaller oscillation than with conventional droop and reach stability fast. Because with the proposed method, the energy stored in the DC-link capacitor is used to maintain system stability without any affecting the performance of the droop controller.
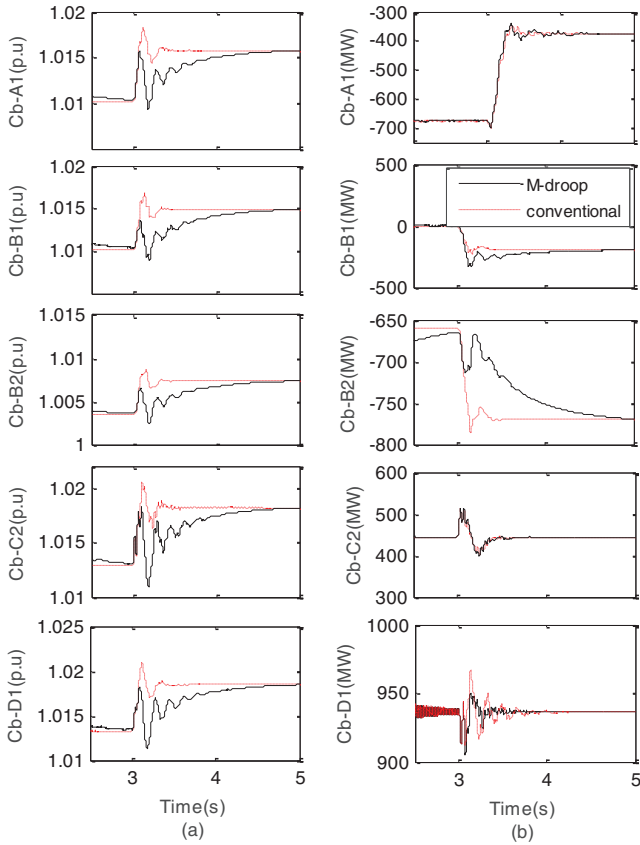
FIGURE 12 (a) DC voltage and (b) power of Cb-A1, Cb-B1, Cb-B2, Cb-C2, and Cb-D1 following 250 MW increasing wind farm 2 generation
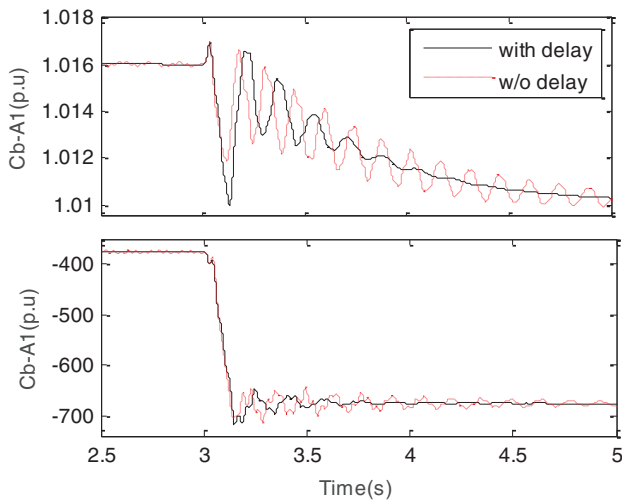

FIGURE 13 DC voltage and power of Cb-A1 following 250 MW reducing wind farm 2 generation

In addition, the frequency of the AC side of Cb-A1 bus is shown in Figure 16. This figure shows the frequency profiles during a three phase short circuit to the ground at the AC side of Cb-A1 bus for 150 ms (3–3.15 s). As shown in Figure 16, with the M-droop method, the frequency oscillations can better damp than with conventional droop and reach stability fast.
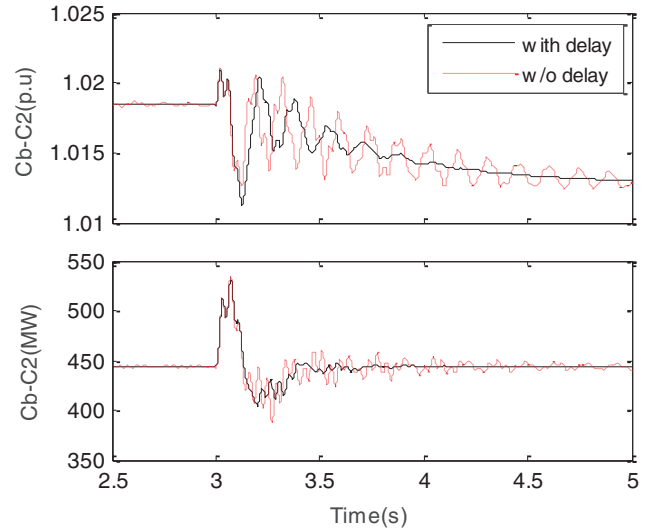

FIGURE 14 DC voltage and power of Cb-C2 following 250 MW increasing wind farm 2 generation
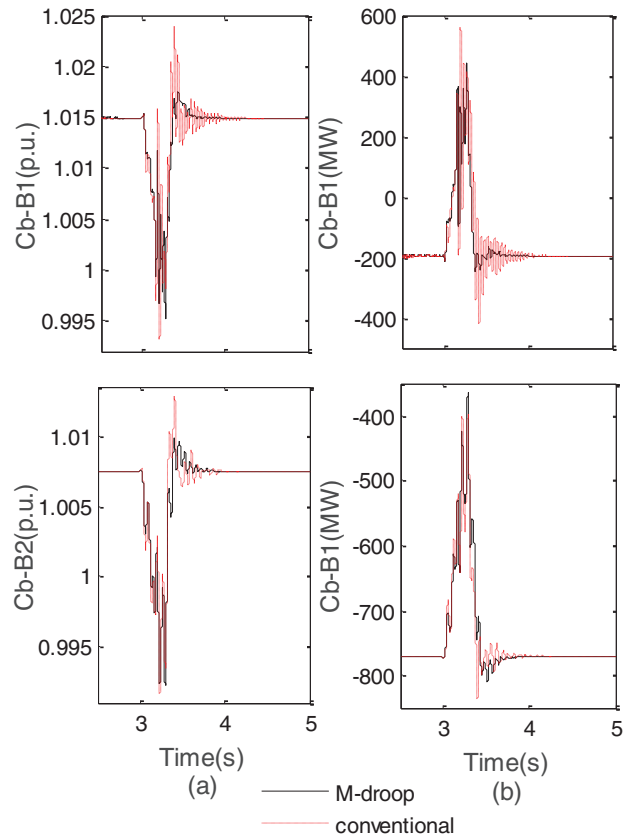

FIGURE 15 (a) DC voltage and (b) power of Cb-B1 and Cb-B2 following a three-phase short circuit to the ground

8 | CONCLUSIONS

One of the main contests in control of HVDC grids is direct voltage regulation. This paper proposed a new control structure for the droop controller called the M-droop controller,
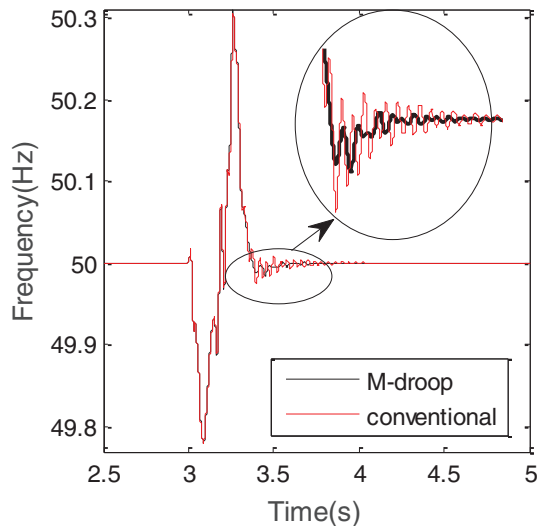
FIGURE 16 The frequency oscillation following a three-phase short circuit to the ground

which can emulate a virtual capacitor behaviour. The conventional DC-PSS can only neutralize a small part of the voltage fluctuations, while, given the presence of the droop controller on the system, it has no proper effect on the volatility of the power. This paper shows that the M-droop controller also provides a part of the capacitance required by the system in addition to damping of the direct voltage oscillations. The feasibility and advantages of the M-droop control strategy have been demonstrated and validated using an accurate simulation model. The compared simulation results under several scenarios related to the DC side of the grid show that the proposed strategy can effectively improve the direct voltage stability.

FUNDING INFORMATION
None

CONFLICT OF INTEREST
The authors confirms that this article content has no conflicts of interest

DATA AVAILABILITY STATEMENT
Data sharing is not applicable to this article as no new data were created or analyzed in this study.

ORCID
Hassan Moradi CheshmehBeigi https://orcid.org/0000-0002-4802-6117

REFERENCES
1. Mohammadi, F., et al.: HVDC circuit breakers: A comprehensive review. IEEE Trans. Power Electron. 36(12), 13726–13739 (2021)
2. Raza, A., Mustafa, A., Alqasemi, U., Rouzbehi, K., Muzzammel, R., Guobing, S., Abbas, G.: HVDC circuit breakers: Prospects and challenges. Appl. Sci. 11, 5047 (2021)
3. Liu, Y., Raza, A., Rouzbehi, K., Li, B., Xu, D., Williams, B.W.: Dynamic resonance analysis and oscillation damping of multiterminal DC grids. IEEE Access 5, 16974–16984 (2017) https://doi.org/10.1109/ACCESS.2017.2740567.
4. Rouzbehi, K., Miranian, A., Luna, A., Rodriguez, P.: DC voltage control and power sharing in multiterminal DC grids based on optimal DC power flow and voltage-droop strategy. IEEE J. Emerg. Sel. Top. Power Electron. 2(4), 1171–1180 (2014)
5. Yogarathinam, A., Chaudhuri, N.R.: Stability-constrained adaptive droop for power sharing in AC-MTDC grids. IEEE Trans. Power Syst. 34(3), 1955–1965 (2019)
6. Sandano, R., Farrell, M., Basu, M.: Enhanced master/slave control strategy enabling grid support services and offshore wind power dispatch in a multi-terminal VSC HVDC transmission system. Renewable Energy 113, 1580–1588 (2017)
7. Wu, D., Tang, F., Dragicevic, T., Guerrero, J.M., Vasquez, J.C.: Coordinated control based on bus-signaling and virtual inertia for islanded DC microgrids. IEEE Trans. Smart Grid 6(6), 2627–2638 (2015)
8. Khorsandi, A., Ashourloo, M., Mokhtari, H.: A decentralized control method for a low-voltage DC microgrid. IEEE Trans. Energy Convers. 29(4), 793–801 (2014) https://doi.org/10.1109/TEC.2014.2329236.
9. Chen, F., Burgos, R., Boroyevich, D., Zhang, W.: A nonlinear droop method to improve voltage regulation and load sharing in DC systems. In: *2015 IEEE First International Conference on DC Microgrids (ICDCM)*, Atlanta, GA, pp. 45–50 (2015)
10. Wang, J., Jin, C., Wang, P.: A uniform control strategy for the interlinking converter in hierarchical controlled hybrid AC/DC microgrids. IEEE Trans. Ind. Electron. 65(8), 6188–6197 (2017)
11. Rouzbehi, K., Zhang, W., Candela, J.I., Luna, A., Rodriguez, P.: Unified reference controller for flexible primary control and inertia sharing in multi-terminal voltage source converter-HVDC grids. IET Gener. Transm. Distrib. 11(3), 750–758 (2017)
12. Shinoda, K., Benchaib, A., Dai, J., Guillaud, X.: Virtual capacitor control: Mitigation of DC voltage fluctuations in MMC-based HVDC systems. IEEE Trans. Power Delivery 33(1), 455–465 (2017)
13. Shinoda, K., Benchaib, A., Dai, J., Guillaud, X.: DC voltage control of MMC-based HVDC grid with virtual capacitor control. In: *2017 19th European Conference on Power Electronics and Applications (EPE'17 ECCE Europe)*, Warsaw, Poland, pp. P. 1–P. 10 (2017)
14. Rakhshani, E., Mehrjerdi, H., Al-Emadi, N., Rouzbehi, K.: On sizing the required energy of HVDC based inertia emulation for frequency control. In: IEEE Power and Energy Society General Meeting, Chicago, IL (2018)
15. Junyent-Ferr, A., Pipelzadeh, Y., Green, T.C.: Blending HVDC-link energy storage and offshore wind turbine inertia for fast frequency response. IEEE Trans. Sustainable Energy 6(3), 1059–1066 (2014)
16. Liu, Y., Green, T.C., Wu, J., Rouzbehi, K., Raza, A., Xu, D.: A new droop coefficient design method for accurate power-sharing in VSC-MTDC systems. IEEE Access 7, 47605–47614 (2019) https://doi.org/10.1109/ACCESS.2019.2909044.
17. Rouzbehi, K., Zhu, J., Zhang, W., Gharehpetian, G.B., Luna, A., Rodriguez, P.: Generalized voltage droop control with the inertia mimicry capability - step towards automation of multi-terminal HVDC grid. In: Proceedings of the International Conference on Renewable Energy Research and Application (ICRERA), Palermo, Italy (2015)
18. Rouzbehi, K., Candela, J.I., Gharehpetian, G.B., Harnefors, L., Luna, A., Rodriguez, P.: Multiterminal DC grids: Operating analogies to AC power systems. Renewable Sustainable Energy Rev. 70, 886–895 (2017)
19. Zhong, C., Zhang, J., Zhou, Y.: Adaptive virtual capacitor control for MTDC system with deloaded wind power plants. IEEE Access 8, 190582–190595 (2020) https://doi.org/10.1109/ACCESS.2020.3032284.
20. Kirakosyan, A., El-Saadany, E.F., Moursi, M.S.E., Acharya, S., Hosani, K.A.: Control approach for the multi-terminal HVDC system for the accurate power sharing. IEEE Trans. Power Syst. 33(4), 4323–4334 (2018) https://doi.org/10.1109/TPWRS.2017.2786702.
21. Montero-Robina, P., Rouzbehi, K., Gordillo, F., Pou, J.: Grid-following voltage source converters: basic schemes and current control techniques to operate with unbalanced voltage conditions. IEEE Open J. Ind. Electron. Soc. 2, 528–544 (2021)
22. Azizi, N., CheshmehBeigi, H.M., Rouzbehi, K.: Optimal placement of direct current power system stabiliser (DC-PSS) in multi-terminal HVDC grids. IET Gener. Transm. Distrib. 14(12), 2315–2322 (2020)

23. Chaudhuri, N.R., Majumder, R., Chaudhuri, B., Pan, J.: Stability analysis of VSC MTDC grids connected to multimachine AC systems. IEEE Trans. Power Delivery 26(4), 2774–2784 (2011)

24. Bergna, G., et al.: An energy-based controller for HVDC modular multilevel converter in decoupled double synchronous reference frame for voltage oscillation reduction. IEEE Trans. Ind. Electron. 60(6), 2360–2371 (2012)

25. Heidary, A., Radmanesh, H., Naghibi, S.H., Samandarpour, S.: Distribution system protection by coordinated fault current limiters. IET Energy Syst. Integr. 2(1), 59–65 (2020)